Journal of Engineering Mathematics **49:** 19–39, 2004.

Water impact of an asymmetric floating wedge

GIORGIO RICCARDI and ALESSANDRO IAFRATI[1]
Department of Aerospace and Mechanical Engineering, Second University of Naples, 81031, Aversa (CE), Italy
[1]*INSEAN, Italian Ship Model Basin, 00128, Rome, Italy*

Received 7 January 2003; accepted in revised form 16 July 2003

Abstract. The flow generated during the early stage of the impact of an asymmetric wedge is here investigated, with the help of a conformal-mapping technique. The wedge is assumed to be initially at rest and floating on a still free surface of an inviscid and incompressible liquid. The study is aimed at understanding the main features of the flow that develops in the vicinity of the apex of the wedge. Due to the inviscid-fluid assumption, a velocity (and pressure) singularity takes place at the apex of asymmetric wedges, which is here removed by reintroducing viscous effects, in terms of the shedding of a wake from the apex. In the present numerical approach, the wake is modelled through point vortices, circulations of which are provided via a suitable Kutta condition. Attention being focused at the early stage of the impact, the free surface is kept during the penetration of the body. This allows the use of an asymmetric extension of Sedov's solution to describe the flow field generated by the wedge entry. Changes induced by the vortical flow on the velocity field and on the pressure distribution on the wedge are discussed.

Key words: asymmetric impact, conformal mapping, slamming, vortex dynamics

1. Introduction

Water impact is a relevant issue in the naval context. As a matter of fact, hydrodynamic loads originated during the water entry may have important consequences in terms of dynamic and structural responses of ships. Beside this rather direct implication, water entry has several connections with the hydrodynamics of high-speed planing craft, as they emerge by viewing the flow generated by a planing hull, when it passes through a cross-plane fixed in space. This aspect is exploited by the so called $2D + t$ (or $2D + 1/2$) approach: studies in this direction have been carried out in [1–3], for instance. In this context, the importance of the asymmetry, in terms of the dynamic stability of the planing craft during maneuvering operations, becomes evident since, depending on the conditions, restoring or capsizing moments can take place.

The water entry of symmetric bodies has been largely investigated in the past, usually within the framework of a potential-flow assumption, with gravity and surface-tension effects also neglected. After the pioneering works of von Kármán [4] and Wagner [5], a self-similar solution for the wedge entry has been derived by Dobrovol'skaya [6]. The flow singularity at the intersection between the body contour and the free surface made the development of numerical algorithms rather challenging [7]. To this purpose, more recently, fully nonlinear numerical solvers have been proposed [8–10] which make use of suitable models in order to cut off the computational domain the jet induced by the flow singularity. In [11] a similar model has been employed to compute the flow and the hydrodynamic forces generated during the impact of two-dimensional and axisymmetric bodies.

An alternative flat-cylinder theory has been proposed by Vorus [12]. In this theory, the geometry is linearized by satisfying the boundary conditions on the horizontal axis, but the

hydrodynamic nonlinearities are fully retained when enforcing the boundary conditions along the axis. By using a slender-body approximation, Savander [2] applied Vorus' theory to the steady planing problem, in order to recover the pressure distribution on the hull and to identify the wetted region.

In spite of the above significant advances in the symmetric impact problem, little is understood about the asymmetric case. The first attempts to solve the potential flow about an asymmetric wedge date back to Garabedian [13] and Borg [14]. More recently, this problem has been addressed by Toyama [15] and by Scolan *et al.* [16]. In [17], the flow generated by the impact of an asymmetric wedge is numerically solved through a fully nonlinear model. However, due to the irrotational-flow assumption, all these studies predict a self-similar solution, with velocity and pressure singularities at the apex of the wedge.

The presence of the geometry singularity makes vorticity production and/or ventilation rather important. A first attempt to address this problem has been provided by Chekin [18], who proposed a model which describes the flow generated by an asymmetric-wedge impact in three different conditions: the flow is attached to the body, the flow is fully detached from one side and the intermediate case, when a closed cavity is formed about the apex. Recently, an approach able to deal with similar flow conditions has been proposed by de Divitiis and de Socio [19]. Therein a limit value of the asymmetry degree is found, beyond which the attached flow solution does not exist.

The vertical water entry of an asymmetric wedge has been deeply investigated by Xu [20], who extended Vorus' theory to account for flow asymmetry. In [3] it is shown that the dynamic moment is strongly related to the characteristics of the flow on the two sides and a systematic analysis is performed for large asymmetry, aimed at evaluating the critical conditions under which a free-surface detachment from the keel can occur. In [21] the same model has been extended to deal with oblique impact and comparisons with experiments are established. The occurrence of ventilation, as a consequence of the pressure singularity at the apex, is investigated when varying wedge geometry and impact velocities.

To gain insights about the main features of the flow field in the vicinity of the wedge apex, the initial stage of the water entry of an asymmetric wedge is here numerically investigated. The wedge is assumed to be initially floating, with a finite submergence of the apex, on an undisturbed liquid surface. The study is carried out within the framework of a potential-flow approximation of an inviscid, incompressible fluid. Owing to these assumptions, a velocity singularity takes place at the apex. This singularity is removed by artificially reintroducing viscous effects in the form of the shedding of a wake from the apex, numerically modelled through a point-vortex approach [22]. The circulation of each vortex is assigned by enforcing an unsteady Kutta condition at the apex and the contribution of the point vortices to the velocity field is computed by using Biot-Savart's law.

Attention being focused at the flow details close to the apex, only the initial stage of the water entry is considered here. This assumption allows us to neglect the effects of the free-surface deformation on the local velocity field and then to use the asymmetric extension of Sedov's solution [23], to describe the basic flow field at each step of the penetration. The motion of the vortices approximating the wake is followed in a Lagrangian way and, at each time step, a new vortex is introduced in a fixed position, close to the apex and inside the fluid domain. The circulation of the new vortex is assigned in such a way that the velocity is finite at the apex of the wedge.

In the following, the original symmetric solution of Sedov is extended to the asymmetric case. Next, the behaviour of the velocity field about the wedge apex is carefully analyzed and

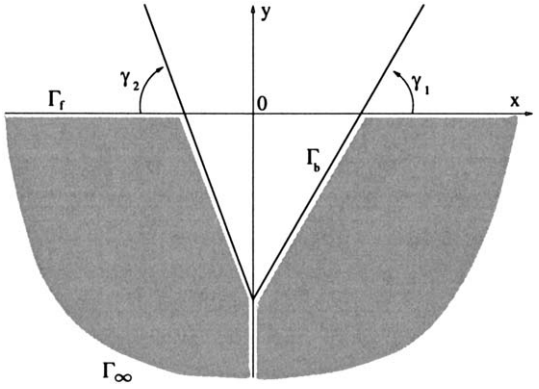

Figure 1. Physical plane $z = x + \mathrm{i}\, y$: the fluid domain Ω is in gray, the wetted part of the wedge and the free surface are indicated by Γ_b and Γ_f, respectively. The fluid domain is closed by the half cylinder Γ_∞, at infinity.

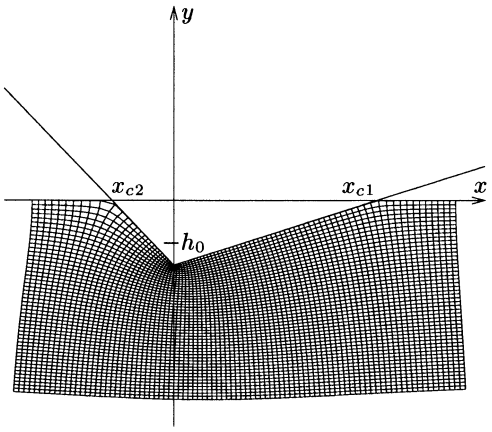

Figure 2. Grid in the physical z-plane corresponding to a Cartesian grid in the ζ-plane, obtained by dividing the segments $(-0{\cdot}60, 1{\cdot}25)$, $(-0{\cdot}801, 0{\cdot}001)$ along the ξ and η axes in 90 and 50 intervals, respectively. The angles γ_1 and γ_2 are 20° and 50°, respectively.

the model adopted for the discretization of the vorticity production is discussed. The model is then applied to simulate the flow generated by the impact of wedges with different degree of asymmetry and the effects of asymmetry on the pressure along the wetted part of the wedge and on the stream function are discussed.

2. Potential flow about an asymmetric floating wedge

2.1. Asymmetric extension of Sedov's solution

The velocity field generated by the water entry of an asymmetric wedge is derived here, within the framework of a potential flow of an inviscid, incompressible fluid. The wedge is assumed to be initially floating on an undisturbed flat liquid surface, with $h_0(t)$ denoting the submergence of its apex at time t. As shown in Figure 1, the deadrise angles of the right and the left sides are denoted by γ_1 and γ_2, respectively. At $t = 0$ the wedge starts to move downward with a given entry velocity $\boldsymbol{V}(t) = \mathrm{i}V(t)$ (hereafter, bold symbols are used for vectors, or complex quantities), where $V(t) = \dot{h}_0(t)$ and $\mathrm{i} = \sqrt{-1}$.

Attention being focused on the flow details about the wedge apex during the early stages of the entry process, the free-surface deformations can be neglected for times t such that $h_0(t)/h_0(0) \simeq 1$. The fluid domain at time t is indicated by $\Omega(t)$ and its boundary $\partial\Omega(t)$ is composed (see Figure 1) of the wetted body contour $\Gamma_b(t)$, of the free surface $\Gamma_f(t)$ and of the half cylinder Γ_∞, at infinity. It is worth noting that, owing to the above simplifying assumption, the wetted body contour Γ_b (hereafter, the dependence on time is omitted) and the free surface Γ_f can be simply derived via geometrical considerations. In particular, with reference to Figure 2, the right intersection between free surface and body is evaluated as $x_{c1}(t) = h_0(t) \cot \gamma_1$ and the left one as $x_{c2}(t) = h_0(t) \cot \gamma_2$, so that the linearized free surface is $\Gamma_f = (-\infty, x_{c2}) \cup (x_{c1}, +\infty)$.

The velocity potential $\phi(x, y; t)$ is governed by the following boundary-value problem:

$$\begin{cases} \nabla^2\phi = 0, & \text{in } \Omega, \\ \nabla\phi \cdot \boldsymbol{\nu} = -V\nu_y, & \text{on } \Gamma_b, \\ \phi = 0, & \text{on } \Gamma_f \cup \Gamma_\infty, \end{cases} \tag{1}$$

where $\boldsymbol{\nu}$ is a vector normal to the body surface. The solution of the boundary-value problem (1) is sought, with the help of a conformal-mapping technique, in terms of the complex velocity potential $\boldsymbol{\mu} = \phi + \mathrm{i}\psi$, where ψ is the stream function. For a symmetric wedge, this boundary-value problem has already been solved in [23]. In the following, this solution is extended to the asymmetric case.

In order to solve the boundary-value problem (1), the fluid domain Ω (in the physical plane $\boldsymbol{z} = x + \mathrm{i}y$) is mapped onto the lower-half of a $\boldsymbol{\zeta}$-plane, with $\boldsymbol{\zeta} = \xi + \mathrm{i}\eta$ and $\eta < 0$. Hence, the physical boundary $\Gamma_b \cup \Gamma_f$ goes onto the real axis $\boldsymbol{\zeta} = \xi + \mathrm{i}0^-$ and the cylinder at infinity Γ_∞ onto the corresponding one in the $\boldsymbol{\zeta}$-plane. The right and left intersection points between the wedge and the free surface are mapped onto the points $\boldsymbol{\zeta} = +1$ and $\boldsymbol{\zeta} = -\delta$, where δ is a positive number that depends, in a way which is discussed below, on the two angles γ_1 and γ_2, with $\delta = 1$ in the symmetric case. With this map, the free surface Γ_f goes onto the segments $\boldsymbol{\zeta} = \xi + \mathrm{i}0^-$ with $\xi < -\delta$ and $\xi > +1$, while the wetted part of the wedge boundary Γ_b goes onto the segment $\boldsymbol{\zeta} = \xi + \mathrm{i}0^-$ with $\delta < \xi < +1$.

The map is built by determining an analytic function $\boldsymbol{g}(\boldsymbol{\zeta})$, the phase of which, along the transformed fluid domain boundary $\boldsymbol{\zeta} = \xi + \mathrm{i}0^-$ with $-\infty < \xi < +\infty$, is equal to the phase of a vector tangent to $\partial\Omega$, at the corresponding point $\boldsymbol{z}(\boldsymbol{\zeta})$ [24], so that

$$\begin{aligned} \boldsymbol{g}(\boldsymbol{\zeta}) &= \mathrm{e}^{\mathrm{i}\gamma_1}\boldsymbol{\zeta}^{(\gamma_1+\gamma_2)/\pi}(1-\boldsymbol{\zeta})^{-\gamma_1/\pi}(\delta+\boldsymbol{\zeta})^{-\gamma_2/\pi} \\ &= |\boldsymbol{g}(\boldsymbol{\zeta})|\mathrm{e}^{-2\mathrm{i}\gamma_1}\mathrm{e}^{\mathrm{i}[\gamma_1(\alpha-\theta)+\gamma_2(\alpha-\beta)]/\pi}, \end{aligned} \tag{2}$$

where $\alpha = \arg(\boldsymbol{\zeta}) \in [0, 2\pi)$, $\beta = \arg(\boldsymbol{\zeta} + \delta) \in [0, 2\pi)$ and $\theta = \arg(\boldsymbol{\zeta} - 1) \in [-\pi, \pi)$. In terms of the function (2), the map can be written as:

$$\boldsymbol{z}(\boldsymbol{\zeta}) = -\mathrm{i}h_0 + \frac{l_1}{w}\int_0^{\boldsymbol{\zeta}} \mathrm{d}\boldsymbol{\chi}\,\boldsymbol{g}(\boldsymbol{\chi}), \tag{3}$$

where $l_1 = h_0/\sin\gamma_1$ is the wetted length of the right side of the wedge and the quantity $w(\gamma_1, \gamma_2)$ is given by:

$$w = \int_0^1 \mathrm{d}\xi\,\xi^{(\gamma_1+\gamma_2)/\pi}(1-\xi)^{-\gamma_1/\pi}(\delta+\xi)^{-\gamma_2/\pi}. \tag{4}$$

It is worth noting that the mapping function (3) has a similarity behaviour with respect to h_0.

In Figure 2, an example of the action of the map (3) on a Cartesian, regular grid in the $\boldsymbol{\zeta}$-plane is shown. The point $\boldsymbol{\zeta} = +1$ is mapped onto the contact point x_{c1} between the free surface and the wedge. Moreover, by enforcing that $\boldsymbol{z}(-\delta) = x_{c2}$, the following condition on the quantity δ is found:

$$\frac{1}{w}\int_0^\delta \mathrm{d}\xi \left(\frac{\xi}{1+\xi}\right)^{\gamma_1/\pi}\left(\frac{\xi}{\delta-\xi}\right)^{\gamma_2/\pi} = r, \tag{5}$$

$r = l_2/l_1 = \sin\gamma_1/\sin\gamma_2$ being the ratio between the wetted lengths of the two sides of the wedge boundary. By combining the relations (4) and (5), the integral equation for δ is obtained:

$$\int_0^{\delta} \mathrm{d}\xi\, \xi^{(\gamma_1+\gamma_2)/\pi}(1+\xi)^{-\gamma_1/\pi}(\delta-\xi)^{-\gamma_2/\pi} = \\ = r\int_0^{1} \mathrm{d}\xi\, \xi^{(\gamma_1+\gamma_2)/\pi}(1-\xi)^{-\gamma_1/\pi}(\delta+\xi)^{-\gamma_2/\pi}, \tag{6}$$

which has solution $\delta = \gamma_1/\gamma_2$, as is shown in Appendix A.

In order to derive the complex velocity potential, the asymptotic behaviour for $|\boldsymbol{\zeta}| \gg 1$ of the function $\boldsymbol{g}(\boldsymbol{\zeta})$ is deduced, starting from the following expansions:

$$(\boldsymbol{\zeta}-1)^{-\gamma_1/\pi} = \boldsymbol{\zeta}^{-\gamma_1/\pi}\left[1+\frac{\gamma_1}{\pi}\frac{1}{\boldsymbol{\zeta}}+\frac{1}{2}\frac{\gamma_1}{\pi}(1+\frac{\gamma_1}{\pi})\frac{1}{\boldsymbol{\zeta}^2}\right]+O(\boldsymbol{\zeta}^{-3}),$$

$$(\delta+\boldsymbol{\zeta})^{-\gamma_2/\pi} = \boldsymbol{\zeta}^{-\gamma_2/\pi}\left[1-\frac{\gamma_2}{\pi}\frac{\delta}{\boldsymbol{\zeta}}+\frac{1}{2}\frac{\gamma_2}{\pi}(1+\frac{\gamma_2}{\pi})\frac{\delta}{\boldsymbol{\zeta}^2}\right]+O(\boldsymbol{\zeta}^{-3}).$$

In the first expansion, the branch with $\theta+2\pi$ of the power $(\boldsymbol{\zeta}-1)^{-\gamma_1/\pi}$ has been considered, so the branch of the function $\boldsymbol{\zeta}^{-\gamma_1/\pi}$ turns out to be the reciprocal of the one of the power $\boldsymbol{\zeta}^{+\gamma_1/\pi}$ that appears at the numerator of the function $\boldsymbol{g}(\boldsymbol{\zeta})$, in Equation (2). By accounting for the solution of the integral equation (6), the asymptotic expansion of the function $\boldsymbol{g}(\boldsymbol{\zeta})$ results:

$$\boldsymbol{g}(\boldsymbol{\zeta}) = 1+\frac{c}{\boldsymbol{\zeta}^2}+O(\boldsymbol{\zeta}^{-3}), \tag{7}$$

where $c = \delta(\gamma_1+\gamma_2)/(2\pi)$. From Equation (7), the asymptotic expansion for large $|\boldsymbol{\zeta}|$ of the map $\boldsymbol{z}(\boldsymbol{\zeta})$ can be evaluated as:

$$z \sim \frac{l_1}{w}\left\{\boldsymbol{\zeta}+\int_1^{\boldsymbol{\zeta}} \mathrm{d}\boldsymbol{\chi}[\boldsymbol{g}(\boldsymbol{\chi})-1]\right\} \sim \frac{l_1}{w}(\boldsymbol{\zeta}-\frac{c}{\boldsymbol{\zeta}})+O(\boldsymbol{\zeta}^{-2}). \tag{8}$$

In Equation (8) and in the following, the symbol $\sim$ means that additional terms, which are constant with respect to the current variable $\boldsymbol{\zeta}$, are dropped.

The complex potential $\boldsymbol{\mu}$ is written as the sum of that of a uniform stream, $\mathrm{i}V\boldsymbol{z}$, and the potential $\boldsymbol{\mu}_r$ of the fluid motion in the wedge frame of reference. Thus, only the potential $\boldsymbol{\mu}_r$ has to be determined, which is real for $\boldsymbol{\zeta} = \xi + \mathrm{i}0^-$ with $-\delta < \xi < +1$ and imaginary along the segments $\xi < -\delta$ and $\xi > +1$. Finally, taking into account the asymptotic behaviour (8) of the map (3), the relative complex potential $\boldsymbol{\mu}_r$ must behave as $-\mathrm{i}l_1V\boldsymbol{\zeta}/w$ for $\boldsymbol{\zeta} \to \infty$, in order to satisfy also the boundary condition along Γ_∞.

The complex potential $\boldsymbol{\mu}_r$ is constructed by introducing the suitable branch of the function $[(1-\boldsymbol{\zeta})(\delta+\boldsymbol{\zeta})]^{1/2}$:

$$\boldsymbol{h}(\boldsymbol{\zeta}) = |1-\boldsymbol{\zeta}|^{1/2}|\delta+\boldsymbol{\zeta}|^{1/2}\mathrm{e}^{\mathrm{i}[\pi+(\theta+2\pi)+\beta]/2},$$

which satisfies the same boundary conditions that hold for $\boldsymbol{\mu}_r$ along the free surface and the wedge. Moreover, for $|\boldsymbol{\zeta}| \gg 1$, $\boldsymbol{h}(\boldsymbol{\zeta})$ behaves as:

$$\boldsymbol{h}(\boldsymbol{\zeta}) = \mathrm{i}(\boldsymbol{\zeta}-s)+O(\boldsymbol{\zeta}^{-1}), \tag{9}$$

with $s = (1-\delta)/2 = (\gamma_2-\gamma_1)/(2\gamma_2)$. Hence, the relative complex potential $\boldsymbol{\mu}_r$ may be written as $\boldsymbol{\mu}_r(\boldsymbol{\zeta}) = -l_1V\boldsymbol{h}(\boldsymbol{\zeta})/w$, leading to the definition of the potential $\boldsymbol{\mu}$:

$$\boldsymbol{\mu}(\boldsymbol{\zeta}) = V\left[\mathrm{i}\boldsymbol{z}(\boldsymbol{\zeta})-\frac{l_1}{w}\boldsymbol{h}(\boldsymbol{\zeta})\right], \tag{10}$$

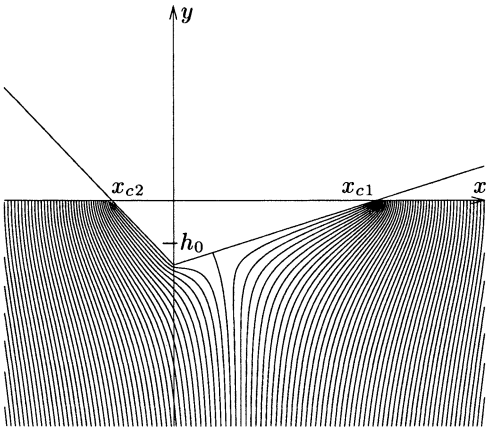

Figure 3. Streamlines in the wedge reference system for the same conditions of Figure 2. A stagnation point lies on the less inclined side of the wedge and the stream turns around the apex, thus leading to the singular behaviour of velocity and pressure at that point. Note also the clustering of the streamlines near the two contact points between wedge and free surface, as induced by the velocity singularities in those points.

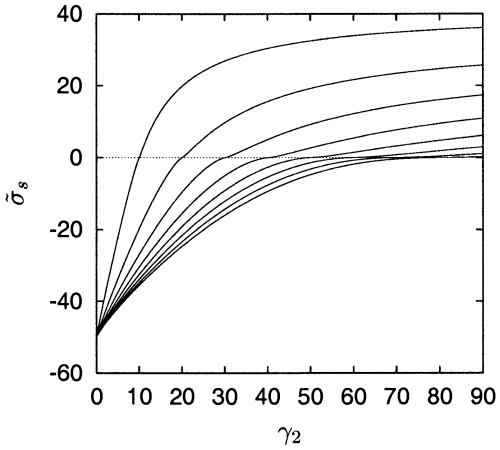

Figure 4. Nondimensional, signed distance $\tilde{\sigma}_s$ from the apex (negative on the left and positive on the right) of the stagnation point vs. γ_2 with $\gamma_1 = 10°$, $20°, \ldots, 80°$, for the fluid motion relative to the wedge. The actual distance σ_s is given by the value of $\tilde{\sigma}_s$ in figure times $l_1/100$ on the right ($\tilde{\sigma}_s > 0$) and $l_2/100$ on the left ($\tilde{\sigma}_s < 0$) of the apex.

which has a similarity behaviour with respect to h_0. The real part ϕ of the complex potential (10) satisfies problem (1).

In Figure 3, the isolines of the relative stream function ψ_r are shown for the flow induced by a wedge with $\gamma_1 = 20°$, $\gamma_2 = 50°$ The presence of a stagnation point on the right side may be observed, as can be derived by analyzing the velocity field. Actually, from the transformation (3) and the form (10) of the complex potential, the conjugate (denoted with overbar) of the complex velocity $\boldsymbol{u}$ in the physical plane is calculated as a function of the transformed variable $\boldsymbol{\zeta}$:

$$\overline{\boldsymbol{u}}(\boldsymbol{\zeta}) = V\left[\mathrm{i} + \frac{\boldsymbol{\zeta} - s}{\boldsymbol{g}(\boldsymbol{\zeta})\boldsymbol{h}(\boldsymbol{\zeta})}\right], \tag{11}$$

which vanishes as $\boldsymbol{\zeta}^{-2}$ for $\boldsymbol{\zeta}$ going to infinity, as a consequence of the asymptotic expansions (7) and (9) for the functions $\boldsymbol{g}$ and $\boldsymbol{h}$.

The velocity field (11) is singular at the apex due to the fact that, in the wedge frame of reference, the stream moves around the apex, turning through an angle greater than π, so the velocity (and the pressure) diverges on the vertex. As noted before, this unphysical behaviour is related to the neglected viscous effects and may be corrected through a generalization of the mathematical model, which includes the shedding of vorticity from the apex, as well as the resulting wake dynamics. The singularities at the contact points, due to the free-surface shape with $\phi = 0$, are responsible for the formation of thin sprays on the two sides of the impacting wedge. The flat-free-surface assumption made in this work does not allow to follow the details of the spray evolution.

From Equation (11), the velocity field relative to the body exhibits a stagnation point on the wedge at the point $\boldsymbol{\zeta} = s + \mathrm{i}0^-$, coinciding with the apex ($s = 0$) only in the symmetric case. For asymmetric configurations, the nondimensional, signed (positive on the right and negative on the left of the apex) distance $\tilde{\sigma}_s$ between the apex itself and the stagnation point is drawn, in percent of the wetted length of the corresponding side, versus γ_2 in Figure 4. It appears that the stagnation point cannot move beyond half the length of the side on which it lies and that, for very sharp wedges, this point is very close to the apex.

The ratio p between pressure and density on the wetted part of the wedge follows from the Bernoulli equation, starting from the potential (10) and the velocity (11). In the transformed plane, the pressure on the body turns out as

$$\begin{aligned} p(\xi) = \; & p_\infty + (\dot{V} + \frac{V^2}{h_0}) \left\{ y + \frac{l_1}{w}[(1-\xi)(\delta+\xi)]^{1/2} \right\} + \\ & + V^2 \left[-\frac{1}{2} \pm \frac{(\pm\xi)^{-(\gamma_1+\gamma_2)/\pi}(\xi - s)\sin\,\gamma_1}{(1-\xi)^{1/2-\gamma_1/\pi}(\delta+\xi)^{1/2-\gamma_2/\pi}} + \right. \\ & \left. - \frac{1}{2}\frac{(\pm\xi)^{-2(\gamma_1+\gamma_2)/\pi}(\xi - s)^2}{(1-\xi)^{1-2\gamma_1/\pi}(\delta+\xi)^{1-2\gamma_2/\pi}} \right], \end{aligned} \tag{12}$$

where the upper signs hold on the right ($0 < \xi < +1$) and the lower ones on the left ($-\delta < \xi < 0$) of the wedge apex. Due to the singularity in the velocity field, the pressure on the wedge also exhibits a singular behaviour at the apex and at the two contact points x_{c1} and x_{c2}. In particular, since $s = 0$ in the symmetric case, the singularity of the pressure at the apex occurs only in the asymmetric case, highlighting a deficiency of the present mathematical modelling of the flow, which does not consider flow separation taking place at that point. In the following this singularity is removed, by accounting for the vortex shedding from the apex, as discussed in Section 3. In Figure 5, for the same flow conditions of Figure 3, $p - p_\infty$ on the wedge is drawn versus the signed curvilinear abscissa σ along the wedge, which is negative to the left and positive to the right of the apex. Almost throughout the wedge surface, the pressure is larger than p_∞, which corresponds to the level 0 in the figure, while, close to the contact points x_{c1} and x_{c2} and to the apex, the pressure quickly falls to $-\infty$. In Section 4 it is shown that the presence of a wake shed from the wedge apex slightly modifies the pressure field in the vicinity of the apex, replacing the singularity at the apex with a finite depression, the intensity and the extent of which depend on the wedge geometry and motion.

2.2. Potential and velocity fields near the singular points

In this section, the behaviour of the map (3) and those of the complex potential (10) and velocity field (11) near the singular points of the transformation itself are investigated. The map (3) has three singular points located at $\boldsymbol{\zeta} = 0$, $\boldsymbol{\zeta} = 1$, and $\boldsymbol{\zeta} = -\delta$. The first singular point, $\boldsymbol{\zeta} = 0$, is the more relevant one for the present analysis: the derivative $\mathrm{d}z/\mathrm{d}\boldsymbol{\zeta} = z' = \boldsymbol{g}$ vanishes and then the velocity (11) diverges, if $s \neq 0$.

In order to evaluate the velocity behaviour near the wedge apex, the variable in the transformed plane is written as $\boldsymbol{\zeta} = 0 + \boldsymbol{\varepsilon}$, with $|\boldsymbol{\varepsilon}| \ll 1$. With this assumption, it may be shown that the map $z(\boldsymbol{\zeta})$ behaves as:

$$z(0+\boldsymbol{\varepsilon}) \simeq -\mathrm{i}h_0 + \frac{\pi}{\gamma_1+\gamma_2+\pi}\frac{l_1}{w}\delta^{-\gamma_2/\pi}\mathrm{e}^{-\mathrm{i}(\gamma_1+2\gamma_2)}\boldsymbol{\varepsilon}^{1+(\gamma_1+\gamma_2)/\pi}, \tag{13}$$

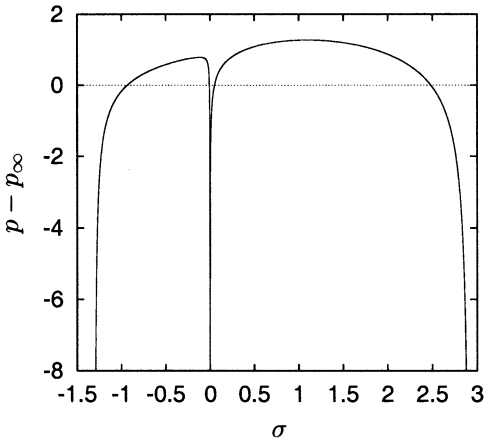

Figure 5. Distribution of $p - p_\infty$ on the wedge vs. the signed curvilinear abscissa σ for the flow due to the motion with $h_0 = 1$, $V = 1$ and $\dot{V} = 0$ of the wedge in Figure 2.

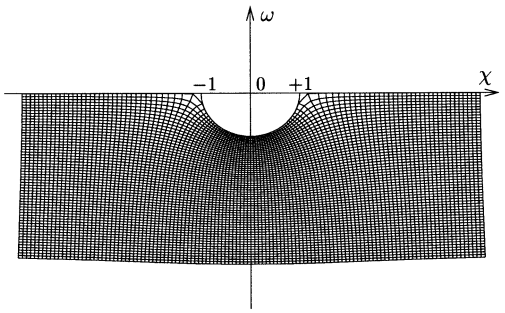

Figure 6. Image in the τ-plane of a cartesian grid in the ζ-plane, obtained by dividing the segments (−1·4, 2) and (−1·301, 0·001) along the axes ξ and η in 120 and 60 intervals, respectively. The geometrical parameters are the same as in Figure 2.

from which the derivative of $\mathrm{d}\zeta/\mathrm{d}z(\zeta)$ becomes:

$$\frac{\mathrm{d}\zeta}{\mathrm{d}z}(0+\varepsilon) \simeq \frac{w}{l_1}\delta^{\gamma_2/\pi}\mathrm{e}^{\mathrm{i}(\gamma_1+2\gamma_2)}\varepsilon^{-(\gamma_1+\gamma_2)/\pi}, \tag{14}$$

where terms that vanish as $\varepsilon \to 0$ have been omitted. This latter estimate points out the divergence of the derivative $\mathrm{d}\zeta/\mathrm{d}z$ in $\zeta = 0$, which leads to a corresponding divergence of the velocity field $u(\zeta)$ around the apex of the body, in asymmetric conditions. The behaviour of the complex potential follows from Equation (10) as:

$$\mu(0+\varepsilon) \sim Vh_0\frac{1}{\sqrt{\delta}}\left(-\frac{s}{w\ \sin\ \gamma_1}\right)\varepsilon, \tag{15}$$

where terms of order $\varepsilon^{(\gamma_1+\gamma_2)/\pi+1}$ have been omitted. In this expansion, ε is multiplied by Vh_0, which depends only on the wedge motion, and by the coefficient $j/\sqrt{\delta}$, j being related to the deadrise angles γ_1 and γ_2 by the following equation:

$$j = -\frac{s}{w\ \sin\ \gamma_1}. \tag{16}$$

This parameter gives the influence of the wedge shape on the vorticity production from the apex; see Equation (25) below. From equation (15), by using the estimate (14), the expansion of the conjugate of the complex velocity in the physical plane as a function of ζ results in:

$$\overline{u}(0+\varepsilon) \simeq V\left[-s\mathrm{e}^{\mathrm{i}(\gamma_1+2\gamma_2)}\delta^{\gamma_2/\pi-1/2}\varepsilon^{-(\gamma_1+\gamma_2)/\pi} + \mathrm{i}\right],$$

where again terms of order ε have been omitted. As mentioned above, in the asymmetric case ($s \neq 0$) the velocity diverges at the apex, while it goes to $-\mathrm{i}V$ in the symmetric one ($s = 0$). When the expansion of the map (13) is taken into account, the velocity diverges as:

$$(z + \mathrm{i}h_0)^{-(\gamma_1+\gamma_2)/(\gamma_1+\gamma_2+\pi)},$$

for $z \to -\mathrm{i}h_0$.

The discussion of the behaviour about the right contact point x_{c1} is carried out by assuming $\boldsymbol{\zeta} = 1 + \boldsymbol{\varepsilon}$, with $|\boldsymbol{\varepsilon}| \ll 1$. The map $\boldsymbol{z}(\boldsymbol{\zeta})$ behaves as:

$$\boldsymbol{z} \simeq x_{c1} + l_1 c' \boldsymbol{\varepsilon}^{(\pi-\gamma_1)/\pi}, \tag{17}$$

where $c' = (\delta + 1)^{-\gamma_2/\pi}\pi/[(\pi - \gamma_1)w]$, where terms of order higher than $\boldsymbol{\varepsilon}^{3/2}$ have been omitted. To the same order of approximation, the corresponding estimate of the complex potential becomes:

$$\boldsymbol{\mu}(1 + \boldsymbol{\varepsilon}) \sim \mathrm{i}Vh_0 \left[-\frac{\sqrt{\delta + 1}}{w \sin \gamma_1} \boldsymbol{\varepsilon}^{1/2} + \frac{c'}{\sin \gamma_1} \boldsymbol{\varepsilon}^{(\pi-\gamma_1/\pi} \right]. \tag{18}$$

An important consequence of the expansions (17) and (18) is that the velocity diverges as:

$$(\boldsymbol{z} - x_{c1})^{-(\pi-2\gamma_1)/[2(\pi-\gamma_1)]},$$

for $z \to x_{c1}$. A similar behaviour, replacing x_{c1} and γ_1 with x_{c2} and γ_2, is found at the contact point on the left side.

3. A model for the vorticity production from the apex

A classical discrete model, able to describe the vortex shedding taking place at the apex of asymmetric wedges [22], is here particularized within the framework of the above conformal-mapping technique. At fixed intervals of time, the vorticity shed from the apex is concentrated in point vortices (Kutta condition), which are placed at a given position, close to the apex and into the fluid domain [25]. During the wedge entry, the point vortices interact with each other and with the body, thus leading to the formation of a wake. It is worth recalling that the basic hypothesis of the present study lies in the flat-free-surface assumption, that is the free surface is not modified by the local velocity field. Under this assumption, Sedov's solution (11), with the actual values of $h_0(t)$ and $V(t)$, is used to evaluate the velocity field induced by the wedge and the free surface on the wake.

In order to significantly simplify the complex potential (11), a new conformal mapping, from the $\boldsymbol{\zeta}$-plane to a $\boldsymbol{\tau}$-plane, is introduced as follows:

$$\boldsymbol{\tau}(\boldsymbol{\zeta}) = \frac{2}{\delta + 1}[\boldsymbol{\zeta} - s - \mathrm{i}\boldsymbol{h}(\boldsymbol{\zeta})], \tag{19}$$

where $\boldsymbol{\tau} = \chi + \mathrm{i}\omega$. The transformation (19) maps the curve $\boldsymbol{\zeta} = \xi + \mathrm{i}0^-$ with $-\delta < \xi < +1$ onto the lower half unitary circle having its center at the origin $\boldsymbol{\tau} = 0$ and the segments with $\xi > 1$ and $\xi < -\delta$ onto the ones $\boldsymbol{\tau} = \chi + \mathrm{i}0^-$ with $\chi > 1$ and $\chi < -1$. In Figure 6, an example of the action of the map (19) on a Cartesian regular grid in the $\boldsymbol{\zeta}$-plane is shown.

The map (19) is easily inverted as:

$$\boldsymbol{\zeta} = \frac{(\delta + 1)\boldsymbol{\tau}^2 - 2(\delta - 1)\boldsymbol{\tau} + (\delta + 1)}{4\boldsymbol{\tau}}, \tag{20}$$

which, for large $|\boldsymbol{\tau}|$, implies $\boldsymbol{\zeta} \sim (\delta + 1)\boldsymbol{\tau}/4$ and, from the asymptotic expansion (8), $\boldsymbol{z} \sim l_1(\delta + 1)\boldsymbol{\tau}/(4w)$. Note that, from Equations (19) and (20), $\boldsymbol{\tau}(s) = -\mathrm{i}$ or $\boldsymbol{\zeta}(-\mathrm{i}) = s$, so that the transformation (19) always maps the stagnation point onto the point $\boldsymbol{\tau} = \mathrm{i}$. Furthermore, the wedge apex $\boldsymbol{\zeta} = 0$ goes to the point

$$\boldsymbol{p} = \frac{\delta - 1}{\delta + 1} - \mathrm{i}\frac{2\sqrt{\delta}}{\delta + 1} = \mathrm{e}^{\mathrm{i}\varphi_g} \tag{21}$$

of the $\boldsymbol{\tau}$-plane, where $\varphi_g \in (\pi, 2\pi)$. From Equation (21), it follows that $\boldsymbol{p} = -\mathrm{i}$ only in the symmetric case, for which $\delta = 1$.

With the help of the transformation (20), the complex potential (11) becomes:

$$\boldsymbol{\mu}(\boldsymbol{\tau}) = \mathrm{i}V\left\{z[\boldsymbol{\zeta}(\boldsymbol{\tau})] - \frac{l_1}{w}\frac{\delta + 1}{4}\frac{\boldsymbol{\tau}^2 - 1}{\boldsymbol{\tau}}\right\}. \tag{22}$$

Such a form is particularly useful for analyzing some of the details of the flow in the frame of reference attached to the body, where the complex potential $\boldsymbol{\mu}_r$ is recovered from Equation (22) by omitting the first term in parentheses, thus having:

$$\boldsymbol{\mu}_r(\boldsymbol{\tau}) = -\mathrm{i}V\frac{l_1}{w}\frac{\delta + 1}{4}\frac{\boldsymbol{\tau}^2 - 1}{\boldsymbol{\tau}}.$$

From this expression, $\boldsymbol{\mu}_r$ turns out to be the same as that of a uniform stream with asymptotic velocity $\mathrm{i}Vl_1(\delta + 1)/(4w)$ impinging on the unit circle. Hence, by exploiting the circle theorem, when a point vortex with circulation Γ_v is introduced in the point $\boldsymbol{\tau} = \boldsymbol{\tau}_v$, the contribution of the vortex itself and of its image have to be added to the original velocity potential, thus yielding

$$\begin{aligned}\boldsymbol{\mu}(\boldsymbol{\tau}) = \ & \mathrm{i}V\left\{z[\boldsymbol{\zeta}(\boldsymbol{\tau})] - \frac{l_1}{w}\frac{\delta + 1}{4}\frac{\boldsymbol{\tau}^2 - 1}{\boldsymbol{\tau}}\right\} + \\ & + \frac{\Gamma_v}{2\pi\,\mathrm{i}}\left[\log(\boldsymbol{\tau} - \boldsymbol{\tau}_v) - \log(\boldsymbol{\tau} - \frac{1}{\overline{\boldsymbol{\tau}}_v})\right].\end{aligned} \tag{23}$$

An important consequence of Equation (23) is that the presence of a point vortex in the flow field does not change the asymptotic behaviour of the velocity field, which still vanishes as $\boldsymbol{\tau}^{-2}$ (or $\boldsymbol{\zeta}^{-2}$), for $\boldsymbol{\tau}$ (or $\boldsymbol{\zeta}$) going to infinity.

To account for the vorticity generation at the apex of asymmetric wedges, a discrete model is used, which consists in the introduction of a new (*nascent*, in the following) vortex in a neighbourhood of the apex at each time step. At the initial time, the position $\boldsymbol{\tau}_1$ and the intensity Γ_1 of the first nascent vortex have to be chosen in a way such that the velocity singularity at the apex disappears. When the complex potential $\boldsymbol{\mu}(0 + \boldsymbol{\varepsilon})$, with $|\boldsymbol{\varepsilon}| \ll 1$, is written as a power series in $\boldsymbol{\varepsilon}$, in order to obtain a velocity field $\overline{\boldsymbol{u}} = \mathrm{d}\boldsymbol{\mu}/\mathrm{d}\boldsymbol{\zeta} \cdot \mathrm{d}\boldsymbol{\zeta}/\mathrm{d}z$ regular at the apex, the first term of the series must be proportional to $\boldsymbol{\varepsilon}^2$, thus avoiding the singular behaviour due to the derivative (14) of the mapping function. Moreover, let $\boldsymbol{\tau} = \boldsymbol{p} + \boldsymbol{w}$, with $|\boldsymbol{w}| \ll 1$, from Equation (20) follows:

$$\boldsymbol{\varepsilon} \simeq -\mathrm{i}\sqrt{\delta}\boldsymbol{w}/\boldsymbol{p},$$

where terms of order $\boldsymbol{w}^2$ have been omitted. As a consequence, in order to avoid terms of order $\boldsymbol{\varepsilon}$ in the expansion of $\boldsymbol{\mu}(0+\boldsymbol{\varepsilon})$, terms of order $\boldsymbol{w}$ have to be avoided in the corresponding expansion of $\boldsymbol{\mu}(\boldsymbol{p} + \boldsymbol{w})$. When the expansion (15) and the above relation between $\boldsymbol{\varepsilon}$ and $\boldsymbol{w}$ are used, the complex potential (23) can be expanded in a neighbourhood of the point $\boldsymbol{\tau} = \boldsymbol{p}$ as follows:

$$\boldsymbol{\mu}(\boldsymbol{p} + \boldsymbol{w}) \sim \left[-\mathrm{i}\overline{\boldsymbol{p}}J + \frac{\Gamma_1}{2\pi\,\mathrm{i}}\left(\frac{1}{\boldsymbol{p} - \boldsymbol{\tau}_1} - \frac{1}{\boldsymbol{p} - 1/\overline{\boldsymbol{\tau}}_1}\right)\right]\boldsymbol{w}, \tag{24}$$

neglecting terms of order $\boldsymbol{w}^2$, where $J = Vh_0 j$ is a real quantity. The second term in parentheses is just the conjugate of the velocity induced by the point vortex on the point $\boldsymbol{p}$ of the cylinder which, thanks to the contribution of the image, is always proportional to $-\mathrm{i}\overline{\boldsymbol{p}}$, for any choice of $\boldsymbol{\tau}_1$. For this reason, the nascent vortex can be placed in an arbitrary position close enough to the apex. In the present calculations, the position of the nascent vortex is chosen as $\boldsymbol{\tau}_1 = (1+d)\boldsymbol{p}$, d being an arbitrary small positive number. The effects of the choice of d on the flow field near the apex are discussed in Appendix B. By imposing that the term of order $\boldsymbol{w}$ in the power series expansion of $\boldsymbol{\mu}(\boldsymbol{p}+\boldsymbol{w})$ vanishes, from Equation (24) Γ_1 follows as:

$$\Gamma_1 = \pi\, J \frac{2d}{d+2} = \frac{\pi}{2} V\, h_0 \frac{\delta - 1}{w\ \sin\ \gamma_1} \frac{2d}{d+2}, \tag{25}$$

where the definition of j (16) is used. Of course, the circulation (25) vanishes for symmetric wedges, *i.e.*, for $\delta = 1$. A more careful analysis of expression (25) reveals that the circulation of the nascent vortex is influenced by three factors: (i) the velocity of the wedge, (ii) its geometry, given by the apex depth h_0 and, via δ and w, by the two deadrise angles γ_1 and γ_2, and (iii) the distance d where the vortex is generated in the $\boldsymbol{\tau}$-plane. This latter factor may appear quite arbitrary, d being a small number which can be assigned without any constraint. Nevertheless, for small values of d (of order 10^{-3} in the present calculations), it follows that $2d = (d+2) \simeq d$, that is the *density* of circulation shed into the wake portion lying between the apex and the point of generation, *i.e.*, Γ_1/d, is quite independent of d. Hence, because the self-induced dynamics of the wake depends only on the density of circulation spread on the wake itself, different values of distance d, provided reasonably small, do not affect the wake motion.

All the above only holds at the initial instant ($t = 0$), when no other vortices are present in the flow field. At the time $t = k\Delta t$, where k is a positive integer, there are k vortices in the field and their contribution to the complex potential must be accounted for, in order to consistently evaluate the circulation of the nascent vortex. In this way, a fourth factor, which influences the vorticity production, comes into play: the effect of the wake itself, which is responsible for a rather complicated feedback between vortex shedding and wake dynamics. The nascent $(k+1)$-th vortex is generated at the same position of the first one, *i.e.*, $\boldsymbol{\tau}_{k+1} = (1+d)\boldsymbol{p}$ is assumed, but in this case the expansion (24) of the complex potential $\boldsymbol{\mu}(\boldsymbol{p}+\boldsymbol{w})$, at the first order in $\boldsymbol{w}$, takes the form:

$$\boldsymbol{\mu}(\boldsymbol{p}+\boldsymbol{w}) \sim \Bigg[\overbrace{-\mathrm{i}\overline{\boldsymbol{p}} V\, h_0 j + \frac{1}{2\pi \mathrm{i}} \sum_{m=1}^{k} \Gamma_m \left(\frac{1}{\boldsymbol{p} - \boldsymbol{\tau}_m} - \frac{1}{\boldsymbol{p} - 1/\overline{\boldsymbol{\tau}}_m} \right)}^{-\mathrm{i}\overline{\boldsymbol{p}} J} + \\ + \frac{\Gamma_{k+1}}{2\pi\ \mathrm{i}} \left(\frac{1}{\boldsymbol{p} - \boldsymbol{\tau}_{k+1}} - \frac{1}{\boldsymbol{p} - 1/\overline{\boldsymbol{\tau}}_{k+1}} \right) \Bigg] \boldsymbol{w},$$

which defines implicitly the new real quantity J. As done for the first nascent vortex, in the above expansion the term in $\boldsymbol{w}$ must vanish to provide a finite value of the velocity at the apex, still obtaining $\Gamma_{k+1} = \pi J 2d/(d+2)$, but in terms of the new value of J. The above procedure, which fixes the position of the nascent vortex and evaluates its circulation in such a way that the velocity remains finite on the wedge apex, is known as the *fixed position method* to enforce the Kutta condition [25].

The vortex dynamics is integrated in time in the physical plane. Toward this aim, the complex velocity is modified in order to exclude the self-induced contribution of each vortex.

Let $z' = \mathrm{d}z/\mathrm{d}\zeta$ and $\zeta' = \mathrm{d}\zeta/\mathrm{d}\tau$, for a point vortex located at $\tau = \tau_v$ (which corresponds to the point ζ_v) the term:

$$\lim_{\tau\to\tau_v}\left(\frac{1}{\tau-\tau_v}\frac{\mathrm{d}\tau}{\mathrm{d}z}-\frac{1}{z-z_v}\right)=-\frac{1}{2}\frac{\zeta'^2(\tau_v)z''(\zeta_v)+\zeta''(\tau_v)z'(\zeta_v)}{[z'(\zeta_v)\zeta'(\tau_v)]^2}$$

is added to the conjugate of the velocity in the physical plane (Routh theorem). As a consequence, the motion of the j-th vortex (for $j = 1, \ldots, k+1$) between $k\Delta t$ and $(k+1)\Delta t$ is simulated by integrating the following equation:

$$\begin{aligned}\dot{\overline{z}} = &\left\{\mathrm{i}V\left[z'(\zeta_j)\zeta'(\tau_j)-\frac{l_j}{w}\frac{\delta+1}{4}\frac{\tau_j^2+1}{\tau_j^2}\right]+\right.\\ &\left.+\frac{1}{2\pi\,\mathrm{i}}\sum_{\substack{m=1\\ m\neq j}}^{k+1}\frac{\Gamma_m}{\tau_j-\tau_m}-\frac{1}{2\pi\,\mathrm{i}}\sum_{m=1}^{k+1}\frac{\Gamma_m}{\tau_j-1/\overline{\tau}_m}\right\}\frac{1}{z'(\zeta_j)\zeta'(\tau_j)}+\\ &-\frac{\Gamma_j}{4\pi\,\mathrm{i}}\frac{\zeta'^2(\tau_j)z''(\zeta_j)+\zeta''(\tau_j)z'(\zeta_j)}{[z'(\zeta_j)\zeta'(\tau_j)]^2}.\end{aligned}\tag{26}$$

In Equation (26), in order to avoid numerical instabilities, each term in the first sum, which gives the velocity induced by the other vortices in the flow field on the j-th one, is desingularized, replacing $1/(\tau_j - \tau_m)$ by $(\overline{\tau}_j - \overline{\tau}_m)/(|\tau_j - \tau_m|^2 + \varepsilon)$, where ε is a small positive number.

4. Numerical results

Numerical simulations of the water-entry flow of asymmetric wedges are performed for several values of the deadrise angles γ_1 and γ_2. As already stated, this study is carried out within the framework of a flat-free-surface assumption. This hypothesis, although drastically simplifying the evaluation of the velocity field, is only valid for a wedge displacement much smaller than the initial apex submergence. For larger values, the mutual interaction between the free surface and the wake is expected to play a very important role.

The wedge, assumed to be at rest initially and floating on an undisturbed liquid surface, is progressively accelerated so that the apex submergence varies as:

$$h_0(t) = h_0(0) + V_0\tilde{t}\left(\frac{t}{\tilde{t}} - 1 + \mathrm{e}^{-t/\tilde{t}}\right),\tag{27}$$

where $\tilde{t}$ is a suitable small time. The time derivative of $h_0(t)$ in Equation (27) approaches a Heaviside function of amplitude V_0, as $\tilde{t} \to 0$. The initial apex submergence $h_0(0)$ and the velocity V_0 are used as length and velocity scales, respectively, leading to an implicit definition of the time scale as $h_0(0)/V_0$. In this scale, the time $\tilde{t}$ is fixed at 10^{-3}. In the numerical calculations, the integration in time is performed with a fixed step $\Delta t = 10^{-5}$, which is found suitable to provide an accurate description of the wake production and of its dynamics during the transient period. Finally, in order to account for the larger and larger vorticity scales taking place during the motion, the desingularization parameter ε is assumed to be linearly growing in time as $\varepsilon(t) = \varepsilon_0 + \dot{\varepsilon}_0 t$. The values of the two constants ε_0 and $\dot{\varepsilon}_0$ depend on the parameters of the simulation, and are usually of the order of 10^{-7} and 10^{-4}, respectively.

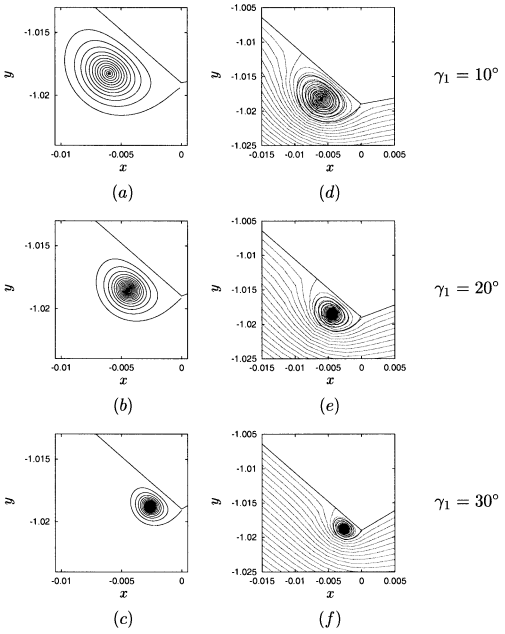

Figure 7. Wake configurations at time $t = 0{\cdot}02$ for different values of γ_1, with $\gamma_2 = 40°$. On the left, wake and body are drawn in an enlarged view around the wake, while, on the right, the corresponding relative streamlines are added.

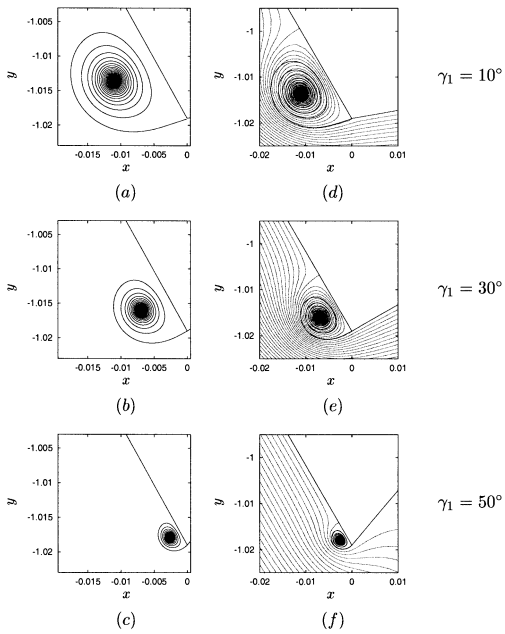

Figure 8. As in Figure 7: wake configurations for the wedges with different values of γ_1, with $\gamma_2 = 60°$.

Without loss of generality, in the present calculations the angle γ_1 is assumed smaller than γ_2. In Figures 7–9 some results are shown when γ_1 is varied for fixed values of γ_2, taken to be 40°, 60° and 80°. Results are presented in terms of wake geometry, on the left, while the iso-contours of the relative stream function $\psi_r = \Im\mathfrak{m}(\boldsymbol{\mu}_r)$ are added, on the right, in order to help in the understanding of the wake dynamics. The numerical solution shows that the wake grows in time, leading to the formation of a quasi-steady vorticity structure, which remains close to the apex on the more inclined part of the wedge. From the analysis of the stream-function fields, the occurrence of a recirculating region, always encompassing the corresponding wake, can be recognized. This region gives rise to a stagnation point, located on side 2, just at the end of the recirculating bubble. There are two other stagnation points: one, due to the Kutta condition, is located just at the apex and another lies on the less inclined side of the wedge (side 1) and is very close, at the initial stage at least, to the one which exists without the wake (see Figure 3). Due to the scales of the figures, this latter stagnation point does not appear in Figures 7–9, except for the last case (Figure 9*f*). In the frame of reference attached to the wedge, the flow coming from the region between the right stagnation point and the apex turns around the recirculating region, up to reaching the most inclined side of the wedge, thus finally moving toward the free surface. In this way, the singularities in the velocity (11) and in the pressure (12), which appears at the apex in the absence of the wake, are removed, leading to a more physical description of the field around the wedge.

For the same flow conditions as shown in Figures 7–9, the total circulation of the wake Γ_w and its time derivative $\dot{\Gamma}_w$ are computed and plotted in Figure 10. Since the circulation Γ_{k+1}

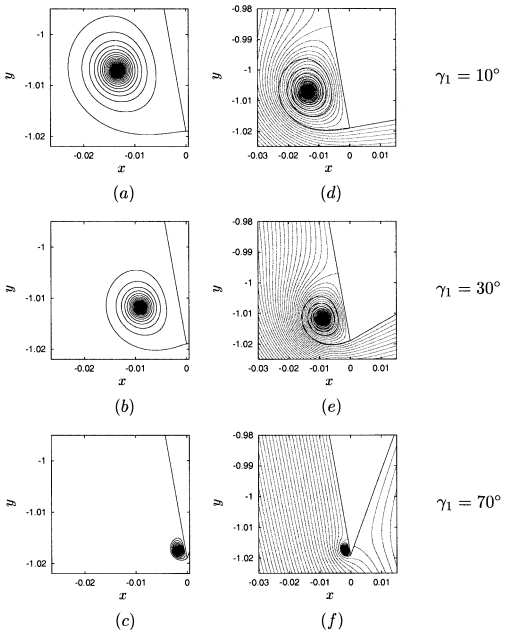

Figure 9. As in Figure 7: wake configurations for the wedges for different values of γ_1, with $\gamma_2 = 80°$.

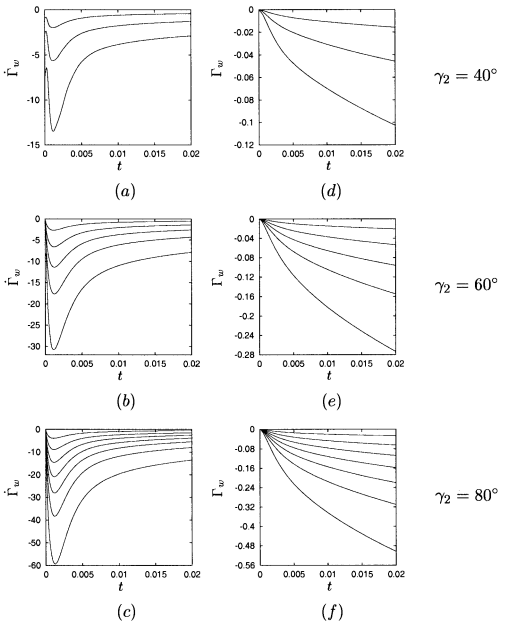

Figure 10. Circulation (right) and its time derivative (left) shed into the wake for several values of γ_2. The angle γ_1 grows, with a step of 10°, from the lowest to the uppermost curve.

of the $(k+1)$-th point vortex is proportional to $\dot{\Gamma}_w$ at the corresponding generation time $k\Delta t$, some interesting insights about the wake dynamics can be derived from the time history of $\dot{\Gamma}_w$, In all calculations shown here, $\dot{\Gamma}_w$, which is always negative, suddenly reaches a minimum and grows subsequently. Hence, the core of the wake is also the region with the larger vorticity density and then it drives the roll-up of weaker vortices shed at a later stage. As a consequence, a relevant stretching is experienced by the intermediate part of the wake, and this makes the integration in time rather challenging, requiring very small time steps to preserve the stability of the numerical calculations. When the long time behaviour of $\dot{\Gamma}_w$ is observed, a conjecture predicts that $\dot{\Gamma}_w$ approaches a constant value. However, it is not completely clear whether such a limit value is negative or zero. This question appears to be relevant in connection with the understanding of the behaviour in time of the stagnation points on the wedge, which is addressed below. At present, the occurrence of such an asymptotic stage for the present mathematical model of the flow is not supported by the numerical results.

The time behaviour of the total circulation Γ_w, whose absolute value grows monotonically, is responsible for a corresponding growth of the distance $|\sigma_2|$ between the apex and the stagnation point on side 2, along which the wake lies. For the same conditions as in Figures 7–9, the time histories of the signed distance σ_2 (negative, when the stagnation point is at the left of the apex) is shown in Figure 11. The behaviour of this distance gives also a measure of the growth of the recirculating region in time which, however, covers only few percents of the wetted length l_2. Concerning the position of the right stagnation point, located at a distance σ_1 from the apex, the relative displacement $(\sigma_1 - \sigma_1^0)/l_1$ with respect to its position σ_1^0 without

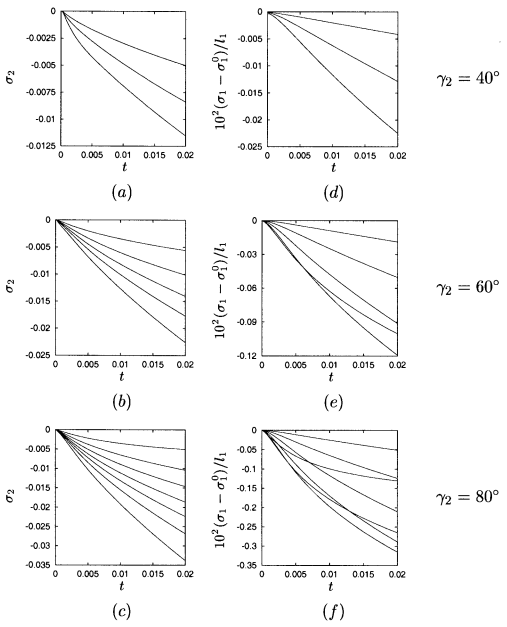

Figure 11. Signed distance σ_2 of the stagnation point on side 2 from the apex (left) and relative displacement $(\sigma_1 - \sigma_1^0)/l_1$ of the stagnation point on side 1 with respect to its position without wake (right). Results for three different values of γ_2 are shown, while the angle γ_1 grows from the lowest to the uppermost curve, with a step of 10°.

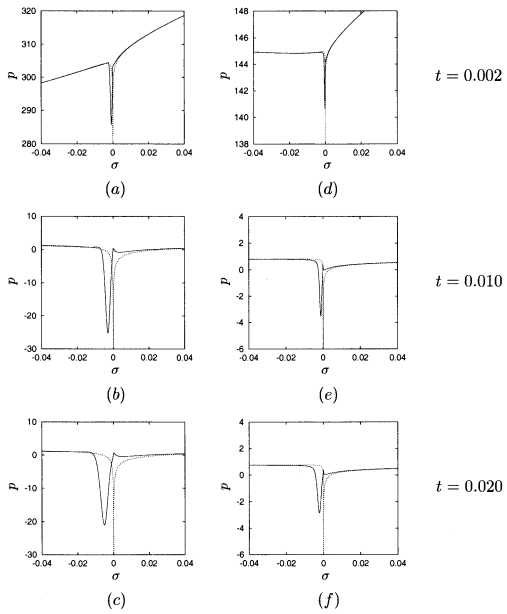

Figure 12. Pressure along the wedge *vs.* the signed curvilinear abscissa σ (negative on the left side and positive on the right one) along the body with (solid line) and without (dashed) the wake. The pressure is assumed zero at infinity. The angle γ_2 is fixed at 40°, while $\gamma_1 = 10°$ in the left column and $\gamma_1 = 30°$ in the right one.

wake is shown *vs.* time on the right-hand side of the same figure. It is worth noting that, at least for the initial stage of the motion, the distance σ_1 grows, also in the presence of the wake, due to the monotonic growth of the apex submergence h_0, given by Equation (27), and to the similarity of the conformal map (3) with respect to h_0. However, Figure 11 shows that, in the presence of the wake, the ratio σ_1/l_1 is always smaller than σ_1^0/l_1, which is constant in time.

To evaluate the pressure field, starting from Equation (12), which is valid in absence of the wake, an additional term, accounting for the vorticity dynamics, is introduced into the unsteady contribution. Hence, at the time $t = k\Delta t$, where k is a positive integer, the time derivative of the complex potential becomes:

$$\partial_t \boldsymbol{\mu}(\boldsymbol{\tau}) = \mathrm{i}\left(\dot{V} + \frac{V^2}{h_0}\right)\left(z - h_0 \frac{\delta + 1}{4\, w\, \sin\, \gamma_1} \frac{\boldsymbol{\tau}^2 - 1}{\boldsymbol{\tau}}\right) + \\ -\frac{1}{2\pi \mathrm{i}} \sum_{m=1}^{k} \Gamma_m \left(\frac{\dot{\boldsymbol{\tau}}_m}{\boldsymbol{\tau} - \boldsymbol{\tau}_m} + \frac{\dot{\overline{\boldsymbol{\tau}}}_m / \overline{\boldsymbol{\tau}}_m^2}{\boldsymbol{\tau} - 1/\overline{\boldsymbol{\tau}}_m}\right),$$

where the time derivative of the k-th vortex position in the $\boldsymbol{\tau}$-plane, $\dot{\boldsymbol{\tau}}_k$, is numerically evaluated by a first-order backward derivative. In Figure 12 the pressure distribution along the wedge with and without the wake is drawn versus the signed curvilinear abscissa σ in a small neighbourhood of the apex, for the flows with $\gamma_2 = 40°$, $\gamma_1 = 10°$ (left column) and $\gamma_1 = 30°$

(right column). It can be seen that the singular behaviour at the apex, occurring in the absence of the wake, disappears and is replaced by a concentrated depression. The extension of such a depression is comparable with the size of the recirculating region, as may be verified by comparing Figure 12*c* with Figure 7*d* and Figure 12*f* with Figure 7*f*. The intensity of the wake-induced depression is larger for the most asymmetric conditions, being roughly in the same ratio as the shed circulations, as can be verified by considering the bottom and the top curves in Figure 10*d*. The time behaviour of the amplitude of such a depression is not monotonic, as can be seen by comparing the three rows in Figure 12. Finally, one may also note the abrupt pressure change about $\sigma = 0$, due to the wake crossing.

5. Conclusions and perspectives

The flow generated by the water entry of a two-dimensional asymmetric wedge, originally floating on a still liquid surface, has been analyzed within the framework of a potential-flow assumption. By focusing attention on the early stage of the flow, free-surface deformations have been neglected, thus allowing to use a generalization of Sedov's solution for the corresponding potential and velocity fields. Owing to the asymmetry, a velocity singularity has been found at the apex, indicating that vortex shedding occurs locally. This deficiency in the mathematical model has been removed by introducing into the flow field point vortices, circulations of which have been assigned in such a way that the velocity singularity at the apex disappears.

For a given law of the entry velocity, the wake generation and its dynamics have been numerically simulated for several combinations of the deadrise angles of the two sides of the wedge and results have been presented in terms of stream function and pressure distribution along the body. The occurrence of a recirculating region has been found, the extension of which grows in time.

Some unresolved questions still remain, in particular with regard to the long-time behaviour of the stagnation points located on the body. For instance, it is not clear if the stagnation point located along the less inclined part of the wedge moves up to the apex and then into the flow field, as can be argued by an intuitive picture of the flow.

An important problem to be addressed in the future concerns the generalization of the present mathematical model, to account for the actual free-surface deformations. Depending on the geometry and on the flow conditions, the mutual interaction between free surface and the vortex wake can be responsible for the occurrence of ventilation and/or flow detachments from the solid body, leading to significant changes in the pressure distribution along the wetted part of the wedge.

Appendix A. Evaluation of the parameter δ

In the following, the parameter δ is determined analytically starting from an evaluation by series of the integrals on the left- and right-hand sides of Equation (6). This is achieved by letting $v' = 1 - \xi/\delta$ and $v'' = 1 - \xi$ in the integrals on the left- and right-hand sides of Equation (6), respectively, yielding

$$\delta(\frac{\delta}{1+\delta})^{\gamma_1/\pi}\int_0^1 \mathrm{d}v' v'^{-\gamma_2/\pi}(1-v')^{(\gamma_1+\gamma_2)/\pi}(1-\frac{\delta}{1+\delta}v')^{-\gamma_1\pi} = \\ = r(\frac{1}{1+\delta})^{\gamma_2/\pi}\int_0^1 \mathrm{d}v'' v''^{-\gamma_1/\pi}(1-v'')^{(\gamma_1+\gamma_2)/\pi}(1-\frac{1}{1+\delta}v'')^{-\gamma_2/\pi}, \tag{A1}$$

in which $\delta/(1+\delta)$ and $1/(1+\delta)$ are both smaller that 1. Let $g_1 = \gamma_1/\pi < 1/2$ and $g_2 = \gamma_2/\pi < 1/2$, by introducing the two coefficients $a_1(\delta) = 1/(1+\delta)$ and $a_2(\delta) = \delta/(1+\delta)$, Equation (A1) becomes:

$$a_2^{g_1+1}\mathcal{F}(g_2, g_1; a_2) = r a_1^{g2+1}\mathcal{F}(g_1, g_2; a_1), \tag{A2}$$

where the function

$$\mathcal{F}(g_1, g_2; a) = \int_0^1 \mathrm{d}v v^{-g_1}(1-v)^{g_1+g_2}(1-av)^{-g_2}, \tag{A3}$$

is introduced. Note that the integrand in Equation (A3) is singular at $v = 0$, but is integrable, since $g_1 < 1/2$. The function (A3) may be evaluated by expanding in Taylor series about $v = 0$ the factor $(1-av)^{-g_2}$:

$$\mathcal{F} = \frac{\Gamma(g_1+g_2+1)}{\Gamma(g_2)}\sum_{k=0}^{\infty}\frac{a^k}{k!}\frac{\Gamma(k+1-g_1)}{(k+1+g_2)(k+g_2)}. \tag{A4}$$

The use of the expansion (A4) in Equation (A2) leads to the following relation:

$$\frac{1}{\Gamma(g_1)}\sum_{k=0}^{\infty}\frac{\Gamma(k+1-g_2)}{(k+g_1)(k+1+g_1)}a_2^{k+1+g_1} = \\ = \frac{r}{\Gamma(g_2)}\sum_{k=0}^{\infty}\frac{1}{k!}\frac{\Gamma(k+1-g_1)}{(k+g_2)(k+1+g_2)}a_1^{k+1+g_2}, \tag{A5}$$

which is a transcendental equation in δ, via $a_1(\delta)$ and $a_2(\delta)$. Equation (A5) is solved numerically by means of a Newton method, for several values of γ_1 and γ_2. The results suggest the simple relation $\delta = \gamma_1/\gamma_2$: here this relation is analytically derived.

Equation (A5) may be rewritten as:

$$\sin\gamma_2\frac{\Gamma(1-g_2)}{\Gamma(g_1)}\Bigg[\frac{1}{g_1(1+g_1)}a_2^{1+g_1}+ \\ +\underbrace{\sum_{k=1}^{\infty}\frac{1}{k!}\frac{(k-g_2)(k-1-g_2)\cdot\ldots\cdot(1-g_2)}{(k+g_1)(k+1+g_1)}a_2^{k+1+g_1}}_{S_2(a_2)}\Bigg] = \\ = \sin\gamma_1\frac{\Gamma(1-g_1)}{\Gamma(g_2)}\Bigg[\frac{1}{g_2(1+g_2)}a_1^{1+g_2}+ \\ +\underbrace{\sum_{k=1}^{\infty}\frac{1}{k!}\frac{(k-g_1)(k-1-g_1)\cdot\ldots\cdot(1-g_1)}{(k+g_2)(k+1+g_2)}a_1^{k+1+g_2}}_{S_1(a_1)}\Bigg], \tag{A6}$$

in which the position $r = \sin\,\gamma_1 \sin\,\gamma_2$ has been used. In the above new form of Equation (A5), the series S_2 and S_1 can be explicitly summed. The series S_2 in the left-hand side of Equation (A6) (the one in the right may be handled in the same way by exchanging the subscript 1 with 2) has a second derivative with respect to a_2 equal to:

$$\begin{aligned}\frac{\mathrm{d}^2 S_2}{\mathrm{d}a_2^2} &= \sum_{k=1}^{\infty} \frac{1}{k!}(k-g_2)(k-1-g_2)\cdot\ldots\cdot(1-g_2)a_2^{k-1+g_1} \\ &= a_2^{-1+g_1}\left[1+\sum_{k=1}^{\infty}\frac{1}{k!}\frac{\mathrm{d}^k}{\mathrm{d}a_2^k}(1-a_2)^{-1+g_2}|_{a2=0}a_2^k\right] - a_2^{-1+g_1} \\ &= a_2^{-1+g_1}(1-a_2)^{-1+g_2} - a_2^{-1+g_1},\end{aligned}$$

leading to the differential problem:

$$\begin{cases} \dfrac{\mathrm{d}^2 S_2}{\mathrm{d}a_2^2} = a_2^{-1+g_1}(1-a_2)^{-1+g_2} - a_2^{-1+g_1} \\ S_2(0) = \dfrac{\mathrm{d}S_2}{\mathrm{d}a_2}(0) = 0, \end{cases}$$

which gives the following expression of the sum S_2:

$$S_2(a_2) = -\frac{1}{g_1(1+g_1)}a_2^{1+g_1} + \int_0^{a_2}\mathrm{d}v'\int_0^{v'}\mathrm{d}v''v''^{-1+g_1}(1-v'')^{-1+g_2}. \tag{A7}$$

Equations (A7) and the analogous one for S_1 are introduced in relation (A6). Both sides of the resulting equation are multiplied by $\Gamma(g_1)\Gamma(g_2)$, so that from the relation $\Gamma(g_1)\Gamma(1-g_1) = \pi/\sin\,\gamma_1$ and the corresponding one for g_2, Equation (A6) is finally rewritten as:

$$\int_0^{a_2}\mathrm{d}v'\int_0^{v'}\mathrm{d}v''v''^{-1+g_1}(1-v'')^{-1+g_2} = \int_0^{a_1}\mathrm{d}v'\int_0^{v'}\mathrm{d}v''v''^{-1+g_2}(1-v'')^{-1+g_1},$$

which can be rearranged in the form:

$$\int_0^1 \mathrm{d}\tilde{v}\int_0^{\tilde{v}}\mathrm{d}v''v''^{-1+g_1}(1-v'')^{-1+g_2} - a_1 B(g_1,g_2) = 0,$$

where B is the Beta function. An integration by parts in the outer integral finally leads to:

$$B(g_1,g_2)\left(\frac{\delta}{1+\delta} - \frac{\gamma_1}{\gamma_2+\gamma_1}\right) = 0,$$

from which it follows $\delta = \gamma_1/\gamma_2$.

Appendix B. Local changes on the low field induced by the nascent vortex

When the position of the first nascent vortex is assumed to be given by $\boldsymbol{\tau}_1 = (1+d)\boldsymbol{p}$, its circulation Γ_1, Equation (25) may be also deduced in a more suggestive way, which enables the analysis of some details of the flow field in a neighbourhood of the apex. Also an empirical criterion for the choice of the distance d follows from that discussion. Actually, in the wedge frame of reference, the complex potential $\boldsymbol{\mu}_r$, in presence of the nascent vortex of circulation Γ_1 at $\boldsymbol{\tau} = \boldsymbol{\tau}_1$, may be written as:

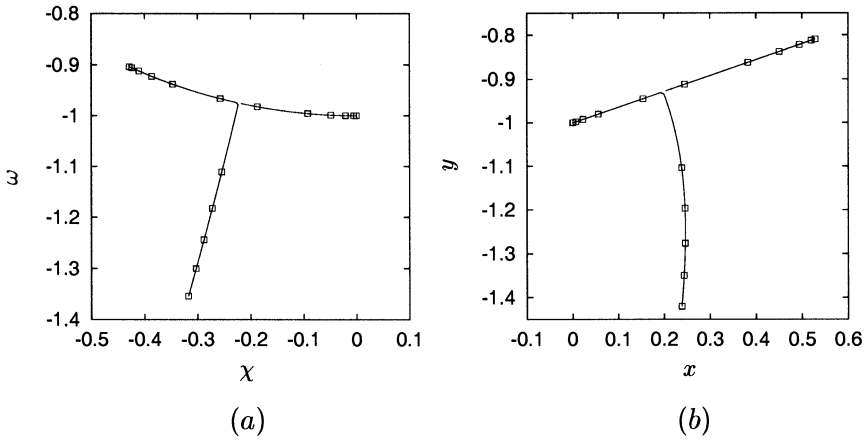

Figure 13. Behaviour of the roots with a physical meaning of Equation (B4) for $\gamma_1 = 20°$, $\gamma_2 = 50°$ and d going from 0 to 0·5, in the $\boldsymbol{\tau}$-plane (a) and in the physical z-plane (b). Symbols are placed along the paths, every $\Delta d = 1/20$.

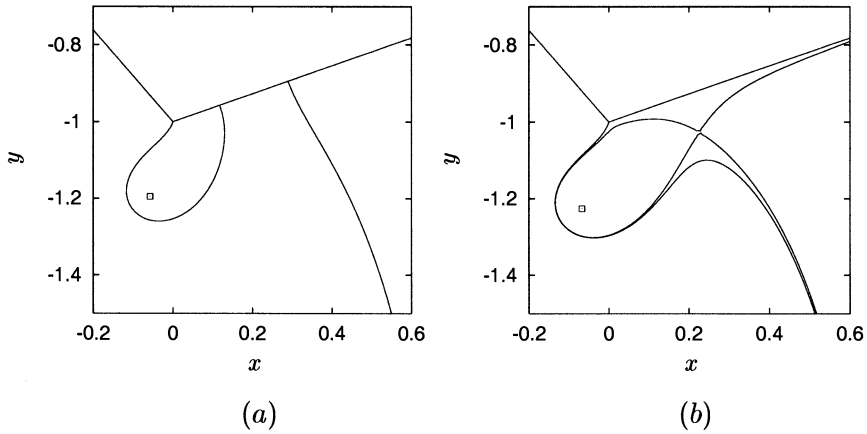

Figure 14. Streamlines through the extremal points in presence of the nascent vortex (square symbol), for the in the wedge reference system with $\gamma_1 = 20°$, $\gamma_2 = 50°$ and $h_0 = 1$. A sub-critical field ($d = 0{\cdot}24 < d_{cr} \simeq 0{\cdot}25$) and a super-critical one ($d = 0{\cdot}27 > d_{cr}$) are shown in (a) and (b), respectively. While in (a) there are three stagnation points all lying on the wedge (one is always located at the apex), in (b) there are only two stagnation points, one at the apex and the other one into the field.

$$\boldsymbol{\mu}_r(\boldsymbol{\tau}) \propto -\mathrm{i}\left\{\boldsymbol{\tau} - \frac{1}{\boldsymbol{\tau}} + c''\left[\log(\boldsymbol{\tau} - \boldsymbol{\tau}_1) - \log\left(\boldsymbol{\tau} - \frac{1}{\boldsymbol{\tau}_1}\right)\right]\right\}, \tag{B1}$$

where $c'' = 2w\Gamma_1/[\pi(\delta + 1)l_1 V]$ is a real constant. Note that the case in which the point vortex is absent can be obtained by letting $\boldsymbol{\tau}_1 = 1/\overline{\boldsymbol{\tau}}_1$, *i.e.*, $d = 0$. When Equation (25) is used for Γ_1, the constant c'' becomes

$$c'' = \frac{\delta - 1}{\delta + 1}\frac{2d}{d + 2}. \tag{B2}$$

When $\boldsymbol{\tau}_1 = (1 + d)\boldsymbol{p}$ is inserted into Equation (B1), the extremal points of the complex potential $\boldsymbol{\mu}_r(\boldsymbol{\tau})$, *i.e.*, the points in which $\mathrm{d}\boldsymbol{\mu}_r/\mathrm{d}\boldsymbol{\tau}$ vanishes, are recovered by the solution of the following fourth-order algebraic equation:

$$\boldsymbol{\tau}^4 - \frac{d^2+2d+2}{d+1}\boldsymbol{p}\,\boldsymbol{\tau}^3 + \left[1 + c''\frac{d(d+2)}{d+1}\boldsymbol{p} + \boldsymbol{p}^2\right]\boldsymbol{\tau}^2 + \\ - \frac{d^2+2d+2}{d+1}\boldsymbol{p}\,\boldsymbol{\tau} + \boldsymbol{p}^2 = 0, \tag{B3}$$

which, for each $d > 0$, has always one root at the point $\boldsymbol{\tau} = \boldsymbol{p}$, *i.e.*, on the wedge apex, if and only if the constant c'' is that given by Equation (B2). This is another way of proving that, if the nascent vortex is placed at $\boldsymbol{\tau}_1 = (1+d)\boldsymbol{p}$, the circulation given by Equation (25) is the only value leading to a finite velocity at the wedge apex, at the initial time.

The other three roots of Equation (B3) are solution of the equation:

$$\boldsymbol{\tau}^3 - \frac{d^2+d+1}{d+1}\boldsymbol{p}\,\boldsymbol{\tau}^2 + \frac{d^2+d+1}{d+1}\boldsymbol{\tau} - \boldsymbol{p} = 0; \tag{B4}$$

depending on the value of d and of $\boldsymbol{p}$, only one or two roots of Equation (B4) have a meaning for the present analysis, the third one being outside the image of the flow field in the $\boldsymbol{\tau}$-plane. The behaviour of these roots versus d in the $\boldsymbol{\tau}$-plane and in the physical one are shown in Figure 13, for an asymmetric wedge with $\gamma_1 = 20°$, $\gamma_2 = 50°$ and $h_0 = 1$. The two roots start, for $d = 0$, one from the body apex and the other from the stagnation point in the absence of the nascent vortex. As d grows, they move along the body, until a critical value d_{cr} is reached, at which the roots merge. For distances d larger than the critical value, only one root of Equation (B4) maintains a physical meaning and is located outside the body.

With regard to the flow in a frame of reference attached to the wedge, in Figure 14 the streamlines through the extremal points are drawn, for the same flow conditions of Figure 13, in the case $d < d_{cr}$ and $d > d_{cr}$, respectively. For subcritical distances (Figure 14*a*), a recirculating region exists along the right-hand side of the wedge contour. For supercritical distances (Figure 14*b*), this region detaches from the body contour and moves below the wedge. An empirical criterion adopted to assign the distance of generation is that d must be smaller than d_{cr}, in order to avoid the presence of an artificial stagnation point into the flow field, close to the apex. It can be shown that the critical distance d_{cr} reduces together with the degree of asymmetry, so the above condition becomes more and more restrictive for γ_1 approaching γ_2.

Acknowledgements

The present activity has been financially supported by the *Ministero dei Trasporti e Navigazione* within the framework of the INSEAN Research Plan 2000 – 02.

References

1. R. Zhao, O.M. Faltinsen and H.A. Haslum, A simplified nonlinear analysis of a high speed planing craft in calm water. In: N. Baird and A. Jeffs (eds.), *Proc. of FAST '97 Conference*. London: Baird Publications (1997) pp. 431–438.
2. B.R. Savander, *Planing Hull Hydrodynamics*. Ph.D. Thesis, Dept. of Naval Architecture and Marine Engineering, University of Michigan (USA) (1997) 158pp.
3. L. Xu, A.W. Troesch and W. Vorus, Asymmetric vessel impact and planing hydrodynamics. *J. Ship Res.* 42 (1998) 187–198.
4. T. von Kármán, The impact of seaplane floats during landing. *NACA TN* 321 (1929) 8pp.
5. H. Wagner, Über Stoß und Gleitvorgänge an der Oberfläche von Flüssigkeiten. *Z. Angew. Math. Mech.* 12 (1932) 192–215.

6. Z.N. Dobrovol'skaya, On some problems of similarity flow of fluid with a free surface. *J. Fluid Mech.* 36 (1969) 805–829.
7. M. Greenhow, Wedge entry into initially calm water. *J. Appl. Ocean Res.* 9 (1987) 214–233.
8. R. Zhao and O.M. Faltinsen, Water entry of two-dimensional bodies. *J. Fluid Mech.* 246 (1993) 593–612.
9. R. Zhao, O.M. Faltinsen and J. Aarnes, Water entry of arbitrary two-dimensional sections with and without separation. In: E. Rood (ed.), *Proc. of 21st Symp. on Naval Hydrodynamics*. Washington: National Academy Press (1996) pp. 118–132.
10. E. Fontaine and R. Cointe, Asymptotic theories of incompressible water entry. In: *High Speed Body Motion in Water, AGARD Rep. 827*.. Neuilly-sur-Seine: Agard Publishers (1997) pp. 25-1–25-9.
11. D. Battistin and A. Iafrati, Hydrodynamic loads during water entry of two-dimensional and axisymmetric bodies. *J. Fluids Struct.* 17 (2003) 643–664.
12. W. Vorus, A cylinder theory for vessel impact and steady planing resistance. *J. Ship Res.* 40 (1996) 89–106.
13. P.R. Garabedian, Oblique water entry of a wedge. *Comm. Pure Appl. Math.* 6 (1953) 157–165.
14. S.F. Borg, Some contributions to the wedge-water entry problem. *J. Eng. Mech. Div.*, Proc. the Am. Soc. Civil Eng. 83 (1957) 1–28.
15. Y. Toyama, Two-dimensional water impact of unsymmetrical bodies. *J. Soc. Naval Arch. Japan* 173 (1993) 285–291 (in Japanese).
16. Y.M. Scolan, E. Coche, T. Coudray and E. Fontaine, Etude analytique et numérique de l'impact hydrodynamique sur des carénes dissimétriques. In: B. Molin (ed.), *Proc. of the 7th Journees de l'Hydrodynamique*. Marseille: Groupe ESIM (1999) pp. 151–164.
17. A. Iafrati, Hydrodynamics of asymmetric wedges impacting the free surface. In: E. Oñate (ed.), *Proc. of the ECCOMAS Conference*. Barcelona: CIMNE (2000) (on CD-rom)
18. B.S. Chekin, The entry of a wedge into an incompressible fluid. *Prikl. Matem. Mekhan.* 53 (1989) 396–404.
19. N. de Divitiis and L.M. de Socio, Impact of floats on water, *J. Fluid Mech.* 471 (2002) 365–379.
20. L. Xu, *A Theory for Asymmetrical Vessel Impact and Steady Planing*. Ph.D. Thesis, Dept. of Naval Architecture and Marine Engineering, University of Michigan (USA) (1998) 128 pp.
21. C. Judge, A.W. Troesch and M. Perlin, Initial water impact at oblique angles. Accepted for publication in *J. Engng. Math.* (2003).
22. G. Riccardi, A. Iafrati and R. Piva, Vorticity shedding from a lentil-shaped body at large incidence in uniform *Meccanica* 29 (1994) 159–173.
23. L.I. Sedov, Floating wedge impact. *Tr. Tsentr. Aerodin. Inst.* 152 (1935) 27–31.
24. H. Kober, *Dictionary of Conformal Representations*. Dover New York (1952) 208 pp.
25. M. Kiya and M. Arie, A contribution to an inviscid vortex-shedding model for an inclined plate in uniform flow. *J. Fluid Mech.* 82 (1977) 223–240.